ORIGINAL ARTICLE

Compost as Green Adsorbent for the Azo Dyes: Structural Characterization and Dye Removal Mechanism

Joanna Kyziol-Komosinska[1] · Agnieszka Dzieniszewska[1] · Sylwia Pasieczna-Patkowska[2] · Anna Kołbus[3] · Justyna Czupioł[1]

Abstract

The study aimed to determine the feasibility of using compost as a 'green adsorbent' for the removal of five anionic azo dyes belonging to the monoazo, disazo and trisazo classes: Direct Red 81 (DR-81), Direct Blue 74 (DB-74), Reactive Blue 81 (RB-81), Reactive Red 198 (RR-198) and Acid Black 194 (ABk-194) from aqueous solutions. The adsorption capacity of the compost was determined using a batch method with initial dye concentrations ranging from 1 to 1000 mg/L. The kinetics of dye removal followed a pseudo-second-order model, indicating chemisorption as the rate-limiting step. The monoazo dyes RB-81, RR-198 and ABk-194 with the smaller molecule size were adsorbed the fastest. The Langmuir and Sips models best fit the adsorption system with maximum adsorption capacities in the range of 12.64 mg/g (RR-198)—20.92 mg/g (ABk-194) and 12.57 mg/g (RR-198)—25.43 mg/g (ABk-194), respectively. The adsorption depended on the dye structure, especially on the ratio of the numbers of proton donors to proton acceptor locations in functional groups. The differences in the adsorption mechanism could be explained by thermodynamic properties such as dipole moments, HOMO–LUMO energy gap, polarizability, electron affinity, ionization potential, electronegativity and chemical hardness obtained by Density Functional Theory.

Graphical Abstract
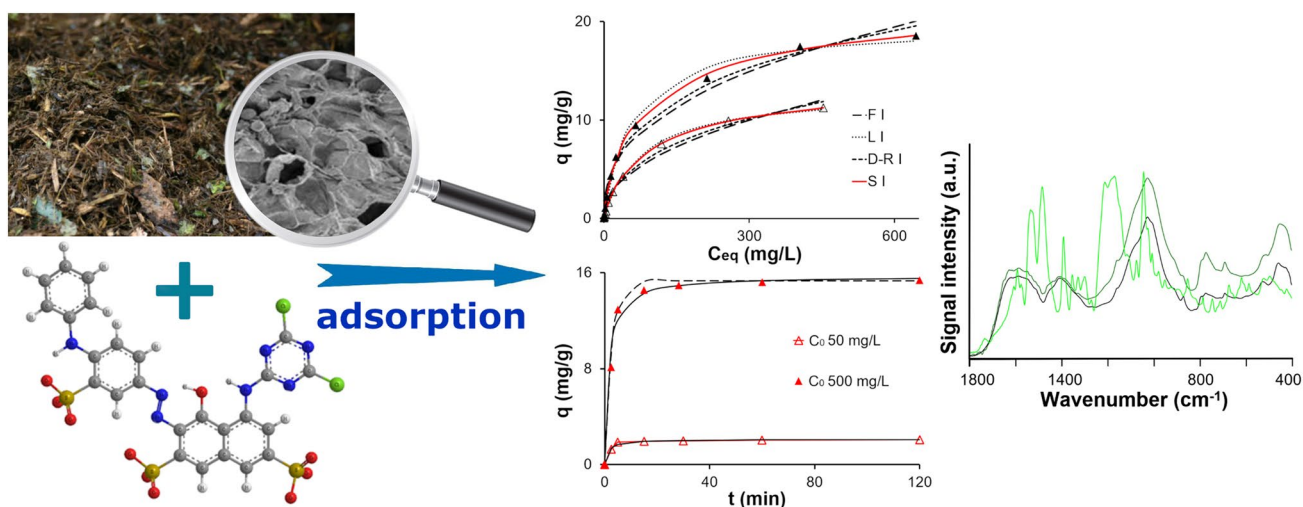
Keywords Compost · Anionic azo dyes · Adsorption isotherms · Kinetics · FTIR spectra · Density Functional Theory

---

Extended author information available on the last page of the article

∂ Springer

Introduction

Life on Earth depends on clean water, as it is one of the essential requirements for all activities, both in the area of everyday life—drinking water and domestic use, and in agricultural production and industrial operations in modern society. According to Directive 2000/60/EC [1], "Water is not a commercial product like any other but, rather, a heritage which must be protected, defended and treated as such". Contamination of natural water sources is therefore a major concern, and maintaining the quality of these sources is a priority for communities. As a result, the Member States of the European Union have made considerable efforts to improve water quality, including through better wastewater treatment.

Synthetic organic dyes are one of the main environmental pollutants due to the large amount of wastewater discharged containing high concentrations of dyes. In addition, the dyeing process often requires large amounts of salt to improve the fixation of the dye on the textile fibers [2], and many dyes also contain heavy metals (e.g. chromium and copper) [3]. Since the first synthetic dye, called mauve, was created by William Perkin in 1856, dyes have been widely used in various industries (textile, leather, paper, printing, cosmetics, pharmaceuticals, food, etc.) to color their products [4].

Dyes can be classified by:

- application—direct, acid, basic, reactive, disperse, vat, etc.,
- ionic species—anionic (direct, acid, and reactive dyes), cationic (all basic dyes), and non-ionic (disperse dyes),
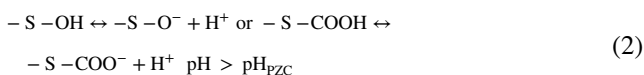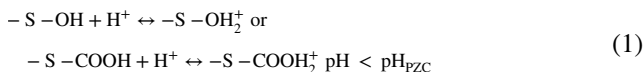- chemical structure—azo, anthraquinone, phthalocyanine, xanthene, nitroso, nitro, etc.

The exact amount of annual production of organic dyes worldwide is difficult to estimate [5] and continues to grow. Overall, more than 1 million tons of dyes are produced annually, of which 50% are textile dyes [6]. In addition, based on the Color Index, there are currently more than 10,000 types of dyes commercially available, including more than 2000 azo dyes [7, 8]. Today, azo dyes (with one or more $R1–N=N–R$ bonds) are the most widely used synthetic dyes in industry, including the dyeing of jeans, cotton and polyester, accounting for at least 50% of the synthetic dyes used worldwide [9, 10]. This also results in their abundance in wastewater [11], as approximately 10–25% of the amount of dye used in the dyeing process is not bound to the textile fibers and can enter the wastewater of these industries [12–14]. In addition, between 2 and 20% of this lost amount is directly discharged as aqueous effluent in various ecosystems [15].

Synthetic dyes alter the aesthetics of natural waters, reduce sunlight penetration, thereby blocking photosynthesis, and increase chemical oxygen demand (COD) in water sources [16]. Even very low levels of these compounds in water (< 1 mg/L) affect the transparency of water bodies because of the high molar absorption coefficients of textile dyes [17]. Many of these dyes are toxic to living aquatic organisms and some are associated with mutagenic, cytotoxic and carcinogenic behavior [8, 18]. Most intermediate metabolites of azo dyes are also aromatic substances, often mutagenic and carcinogenic [19]. Some azo dyes may be incompletely degraded or converted to harmful aromatic amines in the presence of anoxic sediments [20]. In addition, dye-contaminated wastewater typically contains high levels of chemical oxygen demand (COD), biochemical oxygen demand (BOD), total dissolved solids (TDS) and pH [21], often exceeding the limits for effluent standards set by the US EPA [22] and/or national regulations [23]. It is therefore necessary to remove the dyes from the effluent prior to discharge to protect the environment.

Anionic azo dyes are highly soluble and stable in water and are therefore difficult to remove from industrial wastewater by chemical and physical methods [24]. Among the different types of dyes, reactive and acid dyes are the most problematic because they are very difficult to biodegrade and usually pass through conventional treatment systems unaffected [25, 26]. However, the dyes are amphoteric due to the presence of carboxyl, hydroxyl, amino or sulfoxyl functional groups and adsorption has been found to be one of the most effective methods for removing dyes from wastewater compared to the other methods [27]. Although activated carbon is a very good adsorbent, it is also expensive, so new environmentally friendly adsorbents with high adsorption capacity and low cost, capable of operating under neutral pH conditions, are currently being investigated. A very important group of adsorbents are organogenic raw materials such as peat, lignite, oxihumolite, which are rich in humic substances [28–33]. Another group of organogenic adsorbents are materials derived from residues, by-products and composting and thermal treatment (pyrolysis) products from agricultural production [34–37]. These materials are known as "green adsorbents" [38].

Composting is the process of natural degradation of organic waste in the presence of organisms with the ability to recycle it and is an alternative solid waste management system where the organic matter can be recycled into beneficial products. In addition, composts that cannot be used for agronomic purposes (e.g. due to low nutrient levels or above-normal levels of metals and/or phytotoxicity) can be used in wastewater treatment [30, 39]. Composts are safe, stable products, often neutral or slightly alkaline in pH, highly porous and rich in humic substances with surface functional groups of –COOH and –OH. They are positively

charged by surface protonation at a solution pH lower than the pH_{PZC} of the sample, or negatively charged by deprotonation at a solution pH higher than the pH_{PZC} of the sample, according to the following reactions:

$$-S-OH + H^+ \leftrightarrow -S-OH_2^+ \text{ or}$$
$$-S-COOH + H^+ \leftrightarrow -S-COOH_2^+ \quad pH < pH_{PZC} \tag{1}$$

$$-S-OH \leftrightarrow -S-O^- + H^+ \text{ or } -S-COOH \leftrightarrow$$
$$-S-COO^- + H^+ \quad pH > pH_{PZC} \tag{2}$$

and capable of interacting with anionic and cationic species, respectively.

Due to its predominantly negative surface charge, compost interacts more strongly with positively charged compounds (cationic dyes) by electrostatic attraction than with anionic compounds [39–41]. Anionic dyes are mainly bound by adsorbents under acidic conditions [42], and the optimum pH is between 2 and 3 for acidic and reactive dyes [26]. At the same time, both the structure of the anionic dyes and the properties of the compost suggest that they may be bound by other mechanisms (e.g. hydrogen bonding, hydrophobic forces and π–π interactions). Despite its lower adsorption capacity than other efficient organogenic materials (such as low-moor peat) [30], compost can be an attractive adsorbent for the removal of anionic dyes from wastewater. Furthermore, according to Pennanen et al. [43], compost can be used as an adsorbent at lower ambient temperatures, as lower temperatures do not affect its adsorption capacity. The adsorption properties of organogenic materials depend strongly on their origin, while the properties of composts depend on the type of waste and the composting process [44], and therefore require specific studies before being used as adsorbents. In addition, the study of the adsorption capacity of composts and other organogenic adsorbents as a function of their properties allows the database to be improved. Furthermore, the use of composts, especially those with low fertilizer values, for the removal of pollutants from water and wastewater may be a new direction for their management.

The adsorption process is influenced by both adsorbent and contaminant properties. Theoretical calculations provide a good understanding and obtaining a range of information about the adsorbates. Preliminary theoretical analyses allow the prediction of adsorption tendencies. This allows to save time and reagents planned for the experiment, which is consistent with the idea of green chemistry. On the other hand, calculations of physicochemical parameters allow insight into the mechanism of adsorption.

According to the literature, the studies using compost as an adsorbent for dye removal are not numerous and have mostly focused on the removal of cationic dyes from aqueous solutions, with only half as many papers investigating anionic dyes [39]. Additionally, the combination of experimental and computational DFT analysis has also been performed mainly for cationic dyes. To the best of our knowledge, the dyes selected for our research (Direct Red 81, Direct Blue 74, Reactive Blue 81, Reactive Red 198, Acid Black 194) have not been previously analyzed by DFT and none of the research using compost has performed simultaneous analysis of DFT and experimental studies. Therefore, the novelty of this work is the analysis of selected anionic azo dyes with the DFT method, detailed research of the adsorption process on compost combining theoretical and practical approach taking into account the structure and chemical properties of the studied dyes. The use of compost not only meets all the requirements of an economical green adsorbent (effectiveness, cost, abundance and ease of preparation without prior modification), but also combines waste management, environmental remediation and sustainable practices into a single, efficient process.

The scope of the study included: the estimation of the maximum adsorption capacity of the compost for the monoazo, disazo and trisazo dyes and the adsorption rate, the mechanism of dye binding, determination of the equilibrium time of dye adsorption, and the effect of the chemical structure of the dyes (including the number of donors and acceptors of protons in functional groups) on the adsorption capacity of the compost. In addition, a Density Functional Theory (DFT) computational study was performed to determine the optimized geometry and thermodynamic parameters for azo dyes, which helped to explain the differences in their adsorption behavior.

Materials and Methods

Adsorbent

The compost sample was obtained from the stable compost produced from green waste (mown grass, leaves, roots and felled tree branches from parks, squares, recreation and leisure areas) during aeration systems. Composting was carried out in an open-air system with windrows turned periodically for 7 weeks and then matured for 2 months. The compost was produced in a waste treatment plant located in the Upper Silesia region of southern Poland. In the laboratory adsorption experiment, the air-dried, ground, sieved and homogenized fraction < 1 mm was used, with dominant particles in the range of 0.1–100 µm (67.71%).

The main textural, physicochemical and chemical properties of the compost were determined according to the method described by Kyziol-Komosinska et al. [30, 31].

Dyes

Five anionic dyes belonging to the class of monoazo, disazo and trisazo were used in the adsorption study and their characterization is given in Table 1.

Computational Methodology

The optimization of the molecular geometry of the molecules was performed by Density Functional Theory (DFT) calculations using a commercial program Scigress (version FJ 2.7) with the B88-LYP GGA method and the DZVP basis [45, 46]. The DFT method was also used to calculate the dipole moments (the size of the molecule's dipole), the lowest unoccupied molecular orbital (LUMO) energy and the highest occupied molecular orbital (HOMO) energy. The values of log P (the octanol–water partition coefficient) were calculated using the atom typing scheme of Ghose and Crippen [47].

The energy gap was calculated as follows:

$$\Delta E = \left| E_{HOMO} - E_{LUMO} \right| \tag{3}$$

where E_{HOMO} is the energy of the HOMO orbital and E_{LUMO} is the energy of the LUMO orbital.

The values of ionization potential (IP) and electron affinity (EA) were calculated according to the equations [48, 49]:

$$IP = -E_{HOMO} \tag{4}$$

$$EA = -E_{LUMO} \tag{5}$$

where E_{HOMO} is energy of the HOMO orbital and E_{LUMO} is the energy of the LUMO orbital.

Electronegativity (EN) and chemical hardness (η) were given by [48, 49]:

$$EN = \frac{1}{2}(IP + EA) \tag{6}$$

$$\eta = \frac{1}{2}(IP - EA) \tag{7}$$

FT-IR/ATR Analysis

Attenuated Total Reflectance Fourier Transform Infrared (FT-IR/ATR) analysis was performed to determine the nature of the functional groups present in the compost, dyes and compost with adsorbed dyes. The parameters of the analysis are given in the Supplement.

Adsorption Capacity

The adsorption capacity of the compost for dyes was determined in static contact mode (batch method) at room temperature (298 ± 2 K) with initial dye concentration in the range of 1–1000 mg/L and compost dose of 20 g/L and 50 g/L, respectively. The dyes were purchased from Boruta–Kolor (Poland) and used to prepare stock solutions (1000 mg/L) in distilled water. Lower dye concentrations

were obtained by simple dilution. The pH of the stock solution was 8.22 for DR-81, 8.03 for DB-74, 4.97 for RB-81, 4.99 for RR-198 and 5.11 for ABk-194. The solutions with natural pH, without adjustment, were used in the study. Suspensions of compost with dye solution were shaken in a thermostatically controlled shaker at 150 rpm for 300 min to reach equilibrium. The shaking time resulted from the adsorption kinetics studies carried out. After the adsorption procedure, solutions with non-adsorbed dyes were separated by centrifugation for 20 min at 12,850 g using a centrifuge with a JA-20.1 rotor and temperature control unit (Avanti J 25, Beckman Coulter). Samples were not filtered as dyes can be absorbed on the membrane.

The initial (C_0) and equilibrium dye concentrations (C_{eq}) in the solutions were determined by UV/VIS spectrophotometry (Varian Cary 50 Scan spectrophotometer, 1 cm long cell) at the maximum wavelength for each dye (λ_{max}), i.e. 510 nm for DR-81, 582 nm for DB-74, 584 nm for RB-81, 508 nm for RR-198 and 570 nm for ABk-194.

The amount of dye adsorbed (q) and the dye removal efficiency (RE) were calculated from the equations:

$$q = \left(C_0 - C_{eq} \right) \cdot \frac{V}{m} \quad (mg/g) \tag{8}$$

$$RE = \frac{C_0 - C_{eq}}{C_0} \cdot 100\% \tag{9}$$

where V is the volume of the solution (L); m is the weight of adsorbent (g).

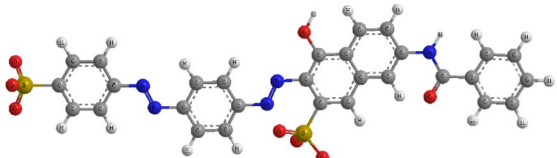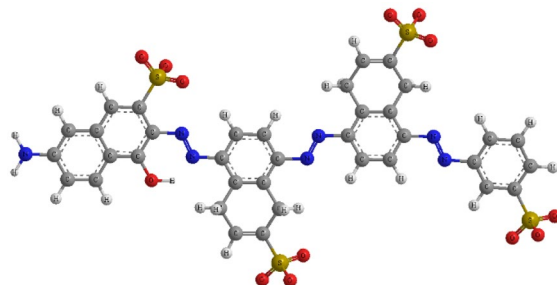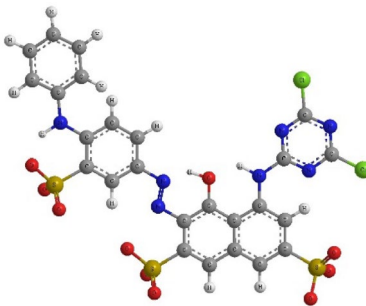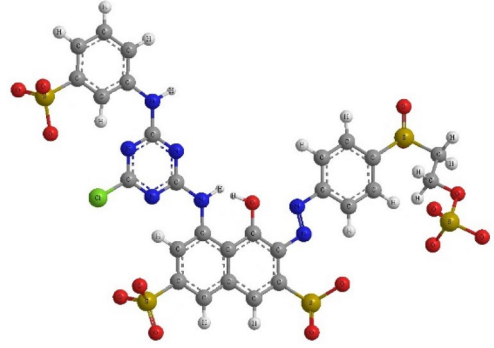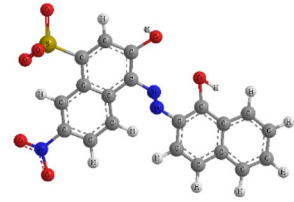The pH of the compost-dye suspension at equilibrium was measured using a pH meter equipped with a glass combination electrode.

Duplicate samples were measured and the standard error of the readings was less than 4%. Control experiments without compost were carried out for all dye solutions to ensure that there was no adsorption of dyes to the walls of the containers.

The relationship between the amount of dye adsorbed on the compost and the concentration of unadsorbed dye in solution at equilibrium can be determined from the adsorption isotherms. The isotherm parameters for the adsorption of the dye ions on the compost were estimated using the Freundlich [50], Langmuir [51] and Dubinin-Radushkevich [52] two-parameter isotherm models and the Sips [53] three-parameter isotherm model (Table S1). The isotherm parameters were estimated by non-linear regression using an algorithm based on the Levenberg–Marquardt method (Statistic ver. 9.0 software).

The effect of the molecular structure of the dyes studied (e.g. the number of donor and acceptor sites in the dyes, the number of aromatic rings and the number of azo bonds) on the experimental adsorption capacity of the compost

Table 1 Characterization of studied dyes

Dye	Chemical formula, C.I., CAS	Characteristics
Direct Red 81 (DR-81)	 $C_{29}H_{19}N_5Na_2O_8S_2$ C.I. 28160 CAS 2610-11-9	$M = 675.6$ g/mol $d = 2.31$ nm pKa $= -3.46$ Class: Dis azo Donor centers: 2 Acceptor centers: 17
Direct Blue 74 (DB-74)	 $C_{36}H_{21}N_7Na_4O_{13}S_4$ C.I. 34146 CAS 33540-94-2	$M = 979.81$ g/mol $d = 2.70$ nm pKa $= -5.78$ Class: Tris azo Donor centers: 3 Acceptor centers: 20
Reactive Blue 81 (RB-81)	 $C_{25}H_{14}Cl_2N_7Na_3O_{10}S_3$ C.I. 18245 CAS 75030-18-1	$M = 808.49$ g/mol $d = 1.83$ nm pKa $= -3.56$ Class: Mono azo Donor centers: 3 Acceptor centers: 12
Reactive Red 198 (RR-198)	 $C_{27}H_{18}ClN_7Na_4O_{16}S_5$ C.I. 18221 CAS 78952-61-1	$M = 984.2$ g/mol $d = 1.96$ nm pKa $= -4.0$ Class: Mono azo Donor centers: 3 Acceptor centers: 23
Acid Black 194 (ABk-194)	 $C_{20}H_{12}N_3NaO_7S$ C.I. 15711 CAS 61931-02-0	$M = 461.38$ g/mol $d = 1.76$ nm pKa $= -2.65$ Class: Mono azo Donor centers: 2 Acceptor centers: 9

M molecular weight; d the largest molecule size

and the maximum Langmuir adsorption capacity, in mg/g and mmol/g, was estimated using Pearson's correlation coefficient.

Study of Kinetics

To understand adsorption/desorption processes, both thermodynamic equilibrium and kinetics must be considered. While thermodynamic data only provide information on the final state of a system, the study of kinetics shows the rate of change of adsorption properties over time [54]. The effect of contact time on the adsorption of all the dyes was studied between 2.5 and 1440 min for C_0 of 50 and 500 mg/L at a compost dose of 20 g/L. The time required to reach equilibrium in the dye solution-adsorbent system was taken into account in the adsorption studies. Two kinetic-based reactions, i.e. Lagergren pseudo-first order (PFO) [55] and pseudo-second order (PSO) [56, 57], were used to find the rate-determining step (Table S2). To describe the adsorption kinetics, the kinetic parameters were estimated by the nonlinear regression method recommended by Tran et al. [58], as the units of the Y and X axes change due to the transformation from nonlinear to linear forms.

The adsorption mechanism for azo dyes-compost systems was investigated using the Morris-Weber (intraparticle diffusion) model (Table S2) [59, 60]. This model allows the determination of whether intraparticle diffusion is the rate-limiting step in the adsorption rate.

In addition to the coefficient of determination (R^2), two non-linear error functions (Table S3) were examined to assess the fit of the kinetic equations and adsorption isotherms to the experimental data [61].

Results and Discussion

Physicochemical Properties of Compost

The textural analysis of the compost by N_2 and H_2O adsorption/desorption showed that the BET surface area was 14.54 and 119.13 m^2/g, respectively, and the porosity determined by the mercury porosimeter was 0.49. The compost contained a high amount of ash, much higher than in biolithes [31]. The chemical composition of the inorganic part of the compost shows that besides Na_2O, MgO and K_2O, SiO_2, Fe_2O_3 and CaO are the main components (Table 2). The extraction test shows that Fe is mainly present as amorphous Fe oxides (37.97% of total Fe), as separate particles or surface coating material of other particles and in complex bonds with organic matter (30.45% of total Fe). According to EU regulation [62], only the Cd content exceeds the limit for an organic fertilizer (1.5 mg/kg dry matter).

The value of the point of zero net charge (pH$_{PZC}$) for the compost was 7.72 and was higher than for the humic substances (3.0–3.5) due to the presence of iron oxides, for which the pH$_{PZC}$ is 8.0–8.5. Iron oxides can modify the surface of organic particles and their properties, including pH$_{PZC}$, and form new adsorption centers. The results showed that at a solution pH lower than 7.72, the surface of compost particles was positively charged and favorable for the adsorption of anionic dyes (Fig. S1). At solution pH > pH$_{PZC}$, the net surface charge is negative because the surface functional groups of the compost (–OH, –COOH) are deprotonated. Although the net charge of the compost can be negative, there are still local positive charges as indicated by

Table 2 The textural, physicochemical and chemical properties of the compost

Textural and physico-chemical properties					
Specific surface area (m^2/g)		Total porosity	pH (H$_2$O)	pH$_{PZC}$	AEC (mmol/g)
Total SSA (H$_2$O)	External SSA (N$_2$)				
119.13	14.54	0.49	7.98	7.72	0.054
Chemical composition (%)						
Ash content	SiO$_2$	Al$_2$O$_3$	Fe$_2$O$_3$	CaO	MgO	K$_2$O	Na$_2$O
69.53	10.82	3.36	4.86	5.24	1.34	2.98	0.21
Heavy metals content (mg/kg)					
Cu	Cd	Cr	Ni	Pb	Zn
172.4	5.55	145.8	15.73	22.17	1112
Leaching of soluble components (mg/L)						
Cu	Cd	Cr	Ni	Pb	Zn	COD
0.23	0.012	0.04	0.05	0.18	1.23	482

the presence of amorphous Fe oxides. The pH_{PZC} is slightly lower compared to the pH_{PZC} of activated teak leaf powder [63] and municipal solid waste compost [64]. The pH of the compost suspension was high (7.98), indicating that the material was in the final stages of the composting process. The anion exchange capacity (AEC) was 0.054 mmol/g and was higher than that of cellulosic biochar at pH 6 and 8 [65]. In addition, AEC decreases with increasing pH of water or soil [66]. The low content of heavy metals in the solutions was observed as an effect of the high pH of the water suspension (pH of about 7.98). In addition, the COD values of the extracts were high, about 482 mgO_2/L, due to dissolved humic acids (Table 2).

The compost has a good buffering capacity—after adding 50 ml of 0.1 M HCl solution to its suspension, the pH only decreased to 7.11 (Fig. S2). It can neutralize acidic wastewater during adsorption without further pH adjustment for already treated water.

FT-IR/ATR Analysis

A detailed description of the FT-IR/ATR spectra can be found in the Supplement (Fig. S3). For better clarity, the FT-IR/ATR spectra of compost, dye and compost with adsorbed dye have been compared in the individual figures.

Study of Kinetics

The effect of the dye structure and its initial concentration in solution (C_0) on the equilibrium time of dye adsorption was observed (Fig. 1). The dye binding process is generally fast and a high level of adsorption is achieved within a short contact time. The equilibrium time was reached within 30 min for all dyes at $C_0 = 50$ mg/L, whereas at $C_0 = 500$ mg/L this time depended on the type of dyes and was 60 min for RR-198, RB-81 and ABk-194 and 300 min for DR-81 and DB-74. The adsorption capacity of the compost reached a plateau after this time for all dyes. The optimum contact time, determined to be 300 min, was used in the adsorption experiments (Fig. 1). A two-step adsorption was observed for both C_0. Adsorption was rapid in the first contact time of 10 min for 50 mg/L and 30 min for 500 mg/L and then increased slowly in the following contact time. During this time, the dyes were bound at 80.5–91.2% and 59.7–95.7% of the total adsorbed amount, respectively. The monoazo dyes RB-81, RR-198 and ABk-194 with the smaller molecule size were adsorbed most rapidly (Table 1).

The dye adsorption rate was high due to the large surface area and pore volume of the compost. As the contact time increased, there were fewer vacant pores available, which slowed the movement of the dye into the pores of the adsorbent and the rate of the adsorption process. The two-step process indicates a rapid, diffusion-controlled
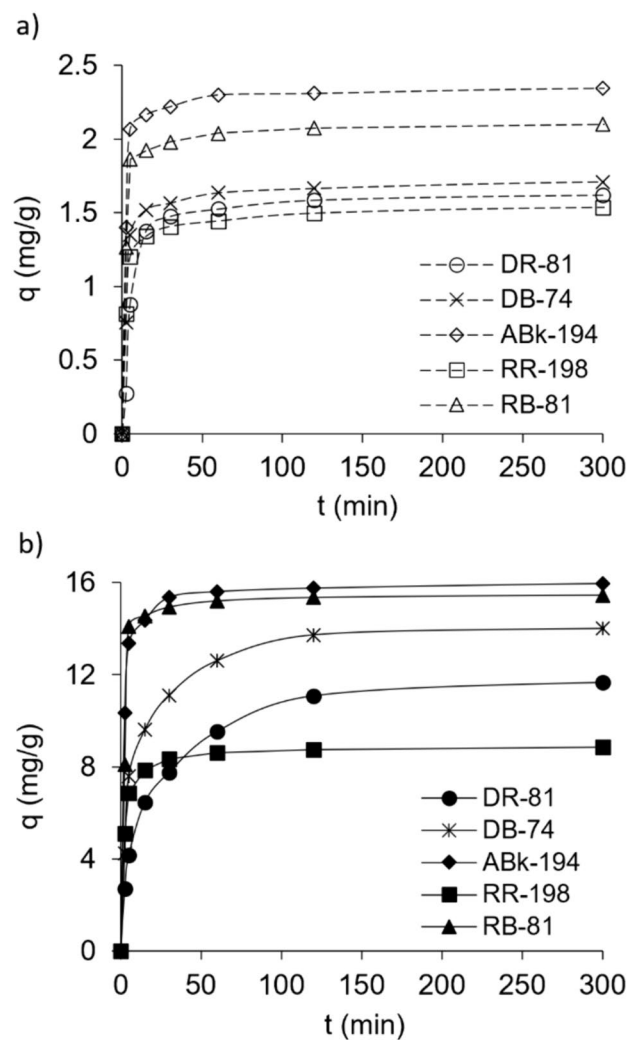

Fig. 1 Effect of contact time on dye adsorption on compost for $C_0 = 50$ mg/L (**a**) and 500 mg/L (**b**)

surface reaction followed by a rate-limiting step that can be explained by various processes, including adsorption to sites with relatively high activation energy and diffusion into the micropores of the compost. A second, slow adsorption step indicates that equilibrium has been reached [67]. The high adsorption rate indicated that the compost had a high efficiency in the removal of azo dyes, which determines the wastewater-compost contact time in the wastewater treatment process in real-world practice.

The pseudo-first order (PFO) and pseudo-second order (PSO) equations are adsorption-reaction models, but the intraparticle diffusion equation is defined as an adsorption-diffusion model. The kinetic models and the Weber-Morris intraparticle diffusion model were used to simulate the experimental data to gain a better understanding of the rate-controlling factors affecting the dye adsorption kinetics.

Regarding the adsorption kinetic models, according to the values of the coefficient of determination and the error functions (SSE and χ^2), both the PFO and PSO models described well the adsorption of all the dyes at their low initial concentration ($C_0 = 50$ mg/L). The adsorption capacity of compost estimated from both equations for all dyes was similar and very close to that determined directly from the laboratory experiment (Table 3). These results indicate that the adsorption of the studied dyes on the compost was dominated by valence forces through electron exchange between the dye anions and positively charged sites on the compost surface, such as iron oxides [20].

At $C_0 = 500$ mg/L, the experimental adsorption data fitted very well only with the PSO model with a very high coefficient of determination ($R^2 > 0.9821$) (Table 3, Fig. 2). Statistical analysis also showed that the PSO model gave better correlations than the pseudo-first-order model. There

is a small difference between the experimental and estimated q values, confirming the applicability of the model [60].

A better pseudo-second-order model fit may indicate the presence of two or more types of adsorption centers on the compost surface, whereas a pseudo-first-order model fit suggests only one type of adsorption site or at least very homogeneous adsorption [26, 64]. Furthermore, the very good PSO fit suggests that the adsorption rate is controlled by chemisorption and the adsorption capacity is controlled by the number of active adsorption sites [68]. It is commonly observed that the removal of dyes from water and wastewater by adsorption on organic-rich material follows this model [24, 56, 64, 69].

The values of the pseudo-second-order rate constants (k_2) decreased with increasing initial dye concentration because the fraction of binding sites available to the dyes decreases with increasing C_0. In addition, a higher value of q correlates with the value of k_2 (Table 3). As C_0 increases, the value of q

Table 3 Kinetics models fitting parameters for the adsorption of azo dyes on compost

Dyes	DR-81		DB-74		RB-81		RR-198		ABk-194	
Pseudo-first and pseudo-second order models										
	PFO	PSO	PFO	PSO	PFO	PSO	PFO	PSO	PFO	PSO
C_0 50 mg/L										
q_{exp}	1.65		1.88		2.10		1.51		2.35	
q_{e1}/q_{e2}	1.598	1.689	1.747	1.947	2.055	2.109	1.478	1.528	2.304	2.364
k_1/k_2	0.1272	0.1055	0.2505	0.2514	0.4081	0.3648	0.3217	0.3441	0.3974	0.3142
h	–	0.301	–	0.953	–	1.756	–	0.805	–	1.623
R^2	0.9812	0.9821	0.9764	0.9736	0.9877	0.9976	0.9828	0.9926	0.9911	0.9934
SSE	0.0632	0.0939	0.1051	0.1029	0.0526	0.0546	0.0368	0.0157	0.0443	0.0627
χ^2	0.1054	0.1055	0.1062	0.1071	0.0268	0.0331	0.0259	0.0136	0.0208	0.0346
C_0 500 mg/L										
q_{exp}	12.45		14.14		15.45		8.85		15.95	
q_{e1}/q_{e2}	11.95	12.71	13.47	14.29	15.30	15.72	8.628	8.921	15.64	16.07
k_1/k_2	0.0442	0.0054	0.1187	0.0012	0.3615	0.0414	0.3347	0.0639	0.4131	0.0482
h	–	0.866	–	2.414	–	12.44	–	5.084	–	10.23
R^2	0.9363	0.9838	0.9391	0.9873	0.9847	0.9887	0.9863	0.9983	0.9875	0.9966
SSE	6.107	1.821	10.40	1.924	1.960	0.2641	0.9731	0.1227	2.824	0.2367
χ^2	2.179	0.492	1.36	0.2931	0.1903	0.1481	0.1271	0.0178	0.1909	0.0556
Intra-particle diffusion model										
	Step 1	Step 2	Step 1	Step 2	Step 1	Step 2	Step 1	Step 2	Step 1	Step 2
C_0 50 mg/L										
K_p	0.3710	0.0277	0.4057	0.0207	0.5059	0.0211	0.3511	0.0209	0.5693	0.0207
C	0.0820	1.296	0.1263	1.451	0.2905	1.856	0.1633	1.274	0.3130	2.104
R^2	0.8331	0.9173	0.9726	0.9349	0.9990	0.9390	0.9891	0.9495	0.9337	0.8540
C_0 500 mg/L										
K_p	1.679	0.6482	2.548	0.5640	6.087	0.1395	3.093	0.1159	6.076	0.1697
C	0.9590	4.183	0.4645	7.822	0.3454	13.94	0.0473	7.579	0.1681	14.08
R^2	0.9944	0.9820	0.9725	0.9494	0.9780	0.8793	0.9984	0.8278	0.9947	0.6956

q_{exp}, q_{e1}, q_{e2} (mg/g); k_1 (1/min); k_2 (g/mg min); h (mg/g min); Kp (mg/g min$^{1/2}$); C (mg/g)

Fig. 2 Time-dependent dyes adsorption on the compost at an initial dye concentration of 50 mg/L and 500 mg/L; (**a**) PFO and PSO models, (**b**) Weber–Morris model; PFO—dashed line, PSO—continuous line
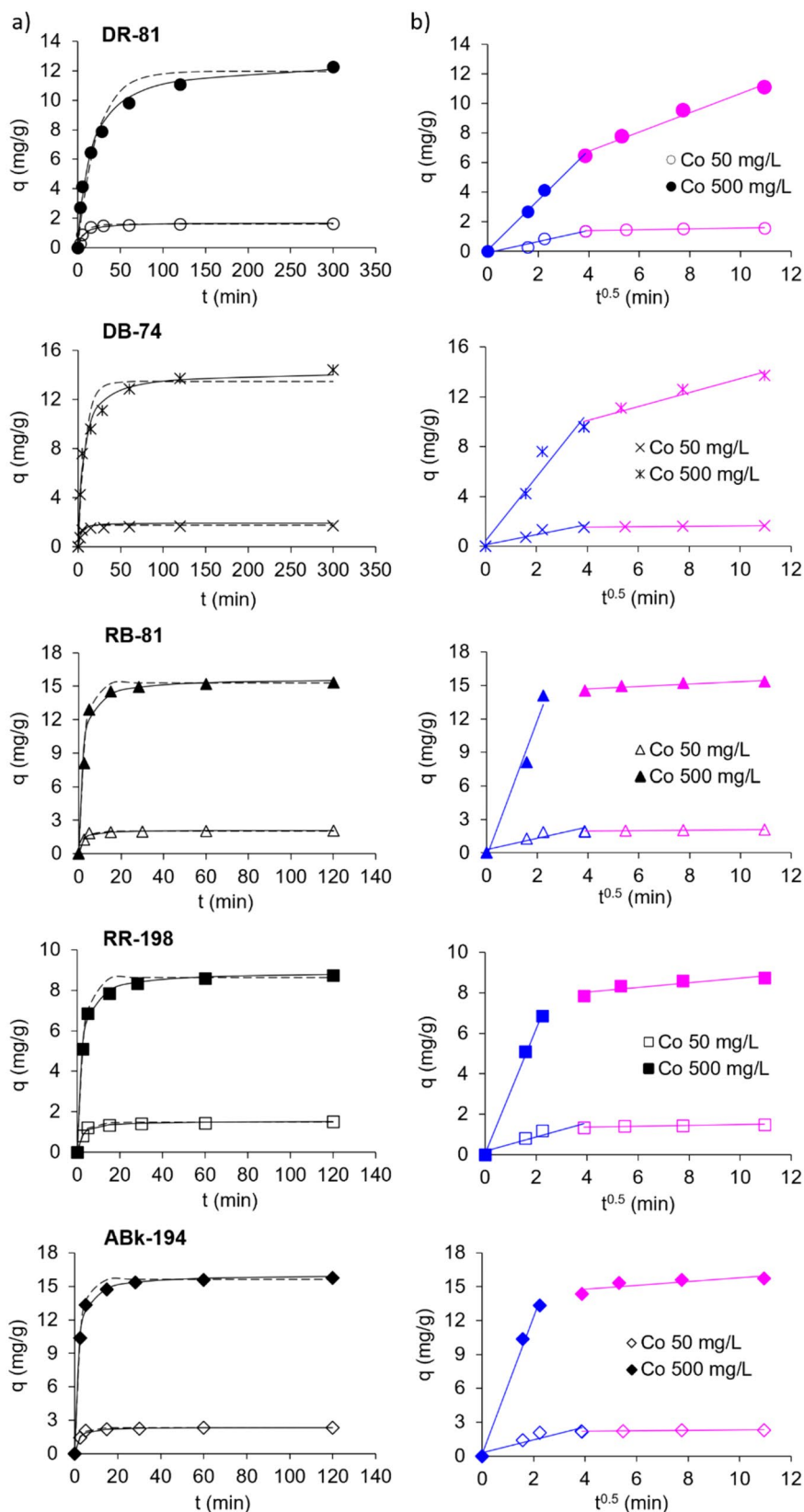
increases and requires a longer time for the system to reach equilibrium, thus decreasing the value of k_2 [70]. This shows that the equilibrium time and adsorption rate are dependent on the amount of dye available, and the higher the initial dye concentration, the longer it takes to reach equilibrium conditions. The initial adsorption rate (h) values indicate that the dye removal rate was fastest for RB-81 and ABk-194, followed by the other dyes. The high initial adsorption rate indicated that the adsorbent had a strong affinity for azo-dye anions. The results also showed that the pseudo-first-order equation fitted the experimental data well for the first 5–15 min of the adsorption process, depending on the type of dye (Fig. 2). According to Ho and McKay [57], the pseudo-first-order model is only applicable to a limited part of the reaction range.

In addition, the intraparticle diffusion model curves did not pass through the origin, indicating that intraparticle diffusion is not the main and only factor determining the adsorption rate and that the adsorption mechanism is very complex [71]. The plots show two diffusion steps that can be attributed to the adsorption stages, where intraparticle diffusion was the rate-limiting step (step 1) and external diffusion (surface adsorption and liquid film diffusion—step 2) can control the adsorption rate [72]. The results also indicated that up to 10–15 min, the rate-determining step was intraparticle diffusion, and beyond that other surface phenomena were involved. Diffusion in solution was probably the limiting step in the process.

Adsorption Capacity of the Compost

The results showed that dye adsorption increased with increasing initial dye concentration due to the strong driving force provided by the concentration gradient [73].

The experimental maximum adsorption capacities of compost for DR-81, DB-74, RB-81, RR-198 and ABk-194 were 7.81, 9.43, 11.22, 5.06 and 12.64 mg/g, respectively, at a compost dose of 50 g/L. A 2.5-fold reduction in the compost dose (to 20 g/L) increased the adsorption capacity from 1.64 (ABk-194) to 1.92 times (RR-198) (Fig. 3a). The dye uptake on the compost was 13.28, 15.97, 18.55, 9.73 and 20.76 mg/g, respectively. Decreasing the adsorbent dosage reduces the number of available active sites, and thus the amount of dye adsorbed per unit mass increases [26]. The order of experimental adsorption affinities to compost is ABk-194 > RB-81 > DB-74 > DR-81 > RR-198 for both compost doses. Expressing the adsorption capacity of the compost in units of mmol/g did not practically change the order of the dyes, only the direct dyes DR-81 and DB-74 replaced each other.

The dye removal efficiency (percentage of dye removal) remained consistently high (95–90%) up to an initial concentration of 25 mg/L and then declined rapidly as the initial concentration increased (Fig. 3b). This effect can be explained by the availability of active sites on the compost surface and their degree of saturation. Therefore, as the dye concentration increases, the saturation of the adsorbent changes, resulting in different removal percentages. At higher concentrations of the dye solution, the removal efficiency decreases because the surface of the adsorbent becomes saturated with dye molecules, making it unable to adsorb further [73]. The measured pH values in the equilibrium dye-compost suspension ranged from 7.95 to 8.37, although the pH of the solutions of the three dyes (RB-81, RR-198, ABk-194) was acidic (Fig. 3c). The pH values resulting from the pH of the compost suspension and the pH of the dye solution were close to the pH of the compost and resulted from the very good buffering properties of the compost. There was no effect of the initial dye concentration on the pH of the equilibrium solution. The pH of the suspensions was also similar for both composts, except for DR-81 and RR-198.

In addition, the pH values in the equilibrium solutions for all dye-compost systems were above the pH_{PZC} of the compost, indicating an overall negative surface charge of the compost particles. At the same time, the pK_a of the dyes was below the pH of the equilibrium solutions, also indicating a negative charge due to the dissociation of their acidic functional groups. Under these conditions, compost cannot bind anionic azo dyes by electrostatic interactions. Electrostatic repulsion significantly affects the adsorption of anionic dyes. However, it should be noted that compost is a heterogeneous adsorbent and the presence of amorphous iron oxides confirms the possibility of occasional binding by electrostatic interactions. In addition, the adsorption capacity of compost for the dyes DR-81, DB-74 and RR-198 (expressed in mmol/g) was lower than its AEC, while that for ABk-194 and RB-81 was higher than its AEC, suggesting that ion exchange may be one of the mechanisms of dye binding.

The molecular structure of the dyes and the structure of the organic matter with aromatic rings and surface functional groups, as described by FT-IR/ATR spectra (Fig. S3), indicated that the adsorption of dyes may also occur via:

- the dipole–dipole interaction or van der Waals attractions between a non-polar part of the dye and the hydrophobic part of the organic matter,
- hydrogen bonds between –OH groups of organic matter and nitrogen, oxygen or hydrogen atoms of dyes,
- π–π and π-hydrogen bonds between the π system of compost and dye molecules with benzene rings containing C=C or naphthyl groups [72, 74].

The results showed that hydrophobic forces between organic matter and dyes are very important for the

Fig. 3 Adsorption of studied azo dyes on compost (**a**), their removal efficiency from solution (**b**), and pH in equilibrium solution (**c**)
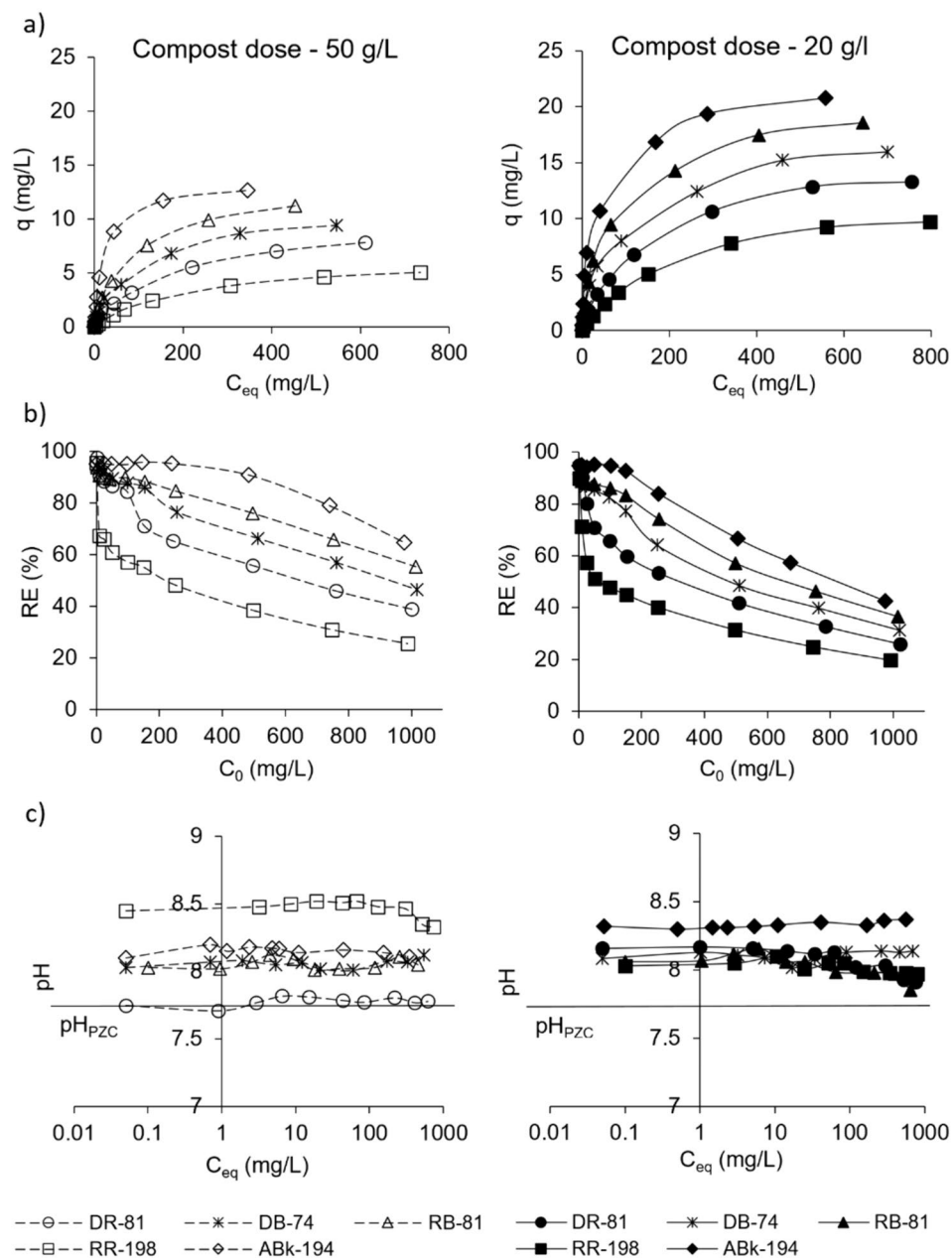
adsorption of dyes [75]. In addition, the structure of the dye molecules and the formation of hydrogen bonds between the –NH₂, –NH- and –OH groups in dyes and the surface functional –COOH and –OH groups in organogenic adsorbents affect their adsorption capacity. According to Reife and Freeman [76], the presence of hydroxyl and nitro groups in the dye molecule increases the adsorption rate, whereas the presence of sulfonic acid groups decreases it. In contrast, Kyziol-Komosinska et al. [31] showed that the adsorption capacity of peat depends on the ratio of donor to acceptor sites in the dyes. Therefore, similar calculations were performed for the azo dye-compost system and confirmed the relationship between

the adsorption capacity of the compost (experimental and estimated from the Langmuir equation) and the ratio of the number of donors to the number of acceptors of the hydrogen atom in the dye functional groups for both compost doses. The highest correlation coefficient was found between the ratio of the number of donors to the number of acceptors and the adsorption capacity of the compost expressed in molar units (Table 4). Moreover, for a constant number of donor centers (DB-74, RB-81 and RR-198 of 3 donor centers) in the dyes, the adsorption capacity of the compost was inversely proportional to the number of acceptor centers (correlation coefficient of 0.9717). On the other hand, no relationship was found between the number

of azo groups in the dyes and the adsorption capacity of the compost.

Furthermore, theoretical values of electronic descriptors as regards all the studied dye molecules: HOMO energy, LUMO energy (DFT method), polarizability (PM6 method), electron affinity (EA), ionization potential (IP), electronegativity (EN), and chemical hardness (η) (Supplementary Materials and Table 5) indicated that chemical reactivity descriptors such as chemical hardness and electronegativity showed that the monoazo dyes (ABk-194, RB-81 and RR-198) were more reactive than the dis- and trisazo dyes (DR-81 and DB-74), which is consistent with the order of the changes in the rate constants obtained from the kinetic study. Electronic density distribution maps for dye molecules (Fig. S4) showed that in the DR-81, DB-74 and RR-198 dyes molecules there are more electron-rich regions and they are more dispersed throughout the whole compared to the ABk-194 and RB-81 dyes molecules. The adsorbent surface is negatively charged, so this charge distribution in the dye molecules could explain a better adsorption of ABk-194 and RB-81 compared to the other three dyes.

Isotherms of Adsorption

The adsorption isotherms of the dyes for both compost doses belong to the L-type isotherms according to the classification of Giles et al. [77], indicating a high affinity between compost particles and dye molecules and the absence of strong competition between dye molecules and water for occupying adsorption active sites (Fig. 4). This suggests that

the adsorption of dyes by organic matter occurs by monolayer formation, with a high affinity between dyes and composts at low concentrations and surface saturation at higher concentrations, which is typical of the Langmuir model [24].

The parameters of the isothermal models estimated by nonlinear regression analysis, the values of the coefficient of determination and the nonlinear error functions are summarized in Table 6, and the fits of the experimental data to the four models are shown in Fig. 4. The results showed that among the isotherms used, the Langmuir (Eq. S2) and Sips (Eq. S5) models showed a very good fit to the behavior of the experimental equilibrium data with $R^2 > 0.99$. From a practical point of view, the Langmuir model is simpler than the three-parameter Sips model and, according to Guerrero-Coronilla et al. [24], is therefore easier to apply and interpret, which has practical implications for engineering design.

The values of maximum adsorption capacity (q_L) estimated from the Langmuir equation were close to or higher than the experimental q values for all dye-compost systems at both compost doses. This observation suggests monolayer adsorption on a homogeneous surface with finite identical adsorption sites. The maximum adsorption capacities can be useful to compare the adsorption capacities of composts for dyes. In addition, the affinity of the compost surface for dyes and the binding energy (K_L) depended on the dye structure and ranged from 0.00454 L/mg (RR-198) to 0.376 L/mg (ABk-194), but there was no effect of compost dose (Table 6). The Sips model gave an improved fit to the experimental data in the higher curvature zone of the adsorption isotherms only for direct dyes (Fig. 4). The use of a third parameter logically improves the quality of the mathematical fit. This model (also called the Langmuir–Freundlich equation) is a combination of the two models and represents systems where an adsorbed molecule can occupy more than one adsorption site. The maximum adsorption capacities (q_S) for the dyes were higher than those obtained using the Langmuir isotherm, and the K_S parameter changed in the same way as the K_L constants of the Langmuir model equation (Table 6). The adsorption capacity obtained from the Sips equation may be more realistic than that obtained from the Langmuir equation [74].

Table 4 Pearson's linear correlation coefficient for adsorption capacity of compost and number of proton donor to acceptor ratio in dyes ($p < 0.05$)

Adsorption capacity of compost	Donor/acceptor (compost dose of 50 g/L)	Donor/acceptor (compost dose of 20 g/L)
q_{max} (mg/g)	0.8045	0.7905
q_L (mg/g)	0.7788	0.8088
q_L (mmol/ g)	0.9671	0.9660

Table 5 The values of electronic descriptors of dyes: HOMO energy, LUMO energy, logP, polarizability, electron affinity, ionization potential, electronegativity, and chemical hardness
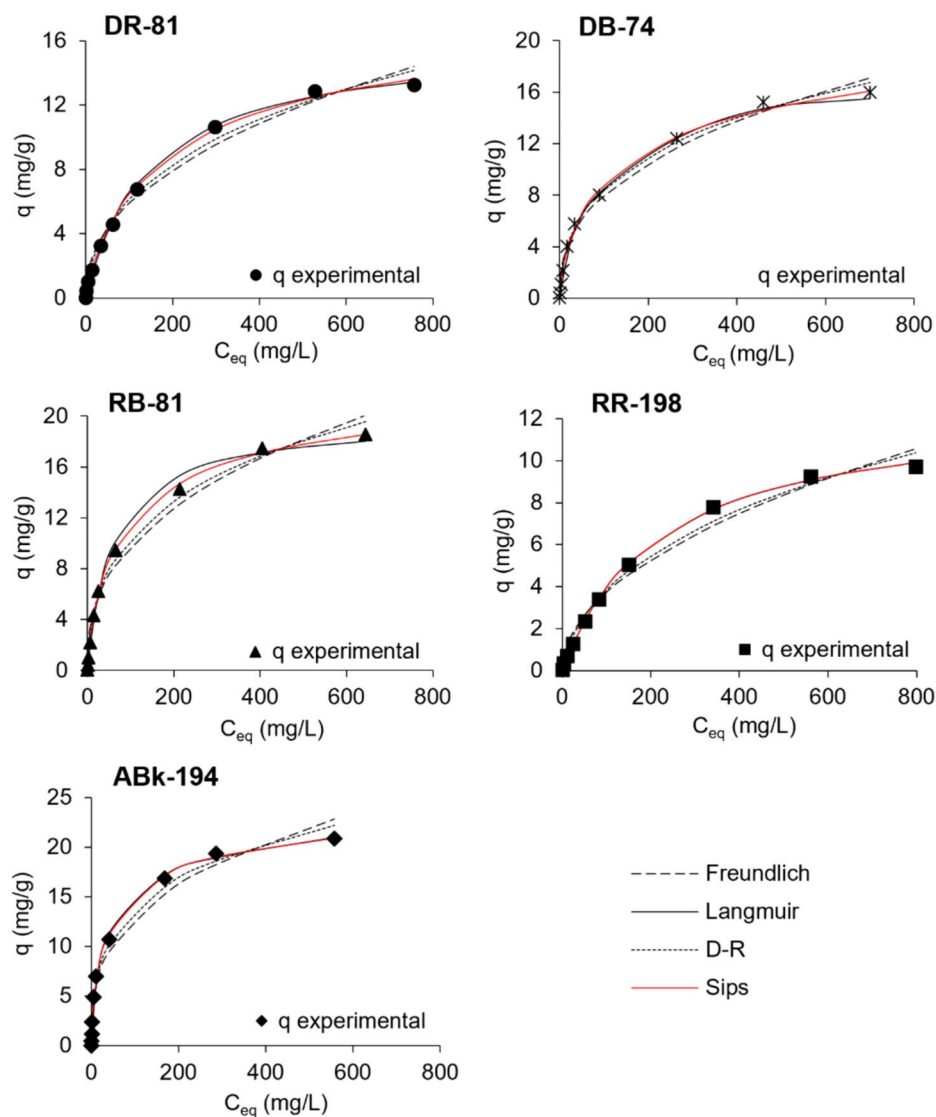
Compound	HOMO energy [eV]	LUMO energy [eV]	Energy gap,ΔE	log P	Polarizability [A^3]	EA [eV]	IP [eV]	EN	(η)
DR-81	− 4.834	− 3.330	1.504	3.647	68.511	3.330	4.834	4.082	0.752
DB-74	− 4.520	− 3.553	0.967	3.291	100.345	3.553	4.520	4.036	0.483
RB-81	− 4.978	− 3.370	1.608	3.533	69.281	3.370	4.978	4.174	0.804
RR-198	− 5.246	− 3.514	1.732	2.071	77.178	3.514	5.246	4.380	0.866
ABk-194	− 5.232	− 3.629	1.603	3.496	43.403	3.629	5.232	4.430	0.802

Fig. 4 Adsorption isotherms of dyes on compost (adsorbent dose 20 g/L)

The results of the error analysis showed that the Freundlich equation (Eq. S1) simulated the adsorption isotherms less well than the Langmuir [78] and Sips models (Table 6). As shown in Fig. 4, the Freundlich model described the experimental data well up to an initial dye concentration of 150 mg/L. The estimated values of $1/n$ were below unity (0.3369–0.5070), indicating that the dyes were easily adsorbed by the compost and the adsorption process was favorable, and a good adsorption capacity of the compost was indicated by an n value above 2. Fitting the adsorption data to the Freundlich isotherm, assuming surface heterogeneity with adsorption sites of different energies and confirming the porous character of the compost, indicates that the adsorption was heterogeneous and not limited to monolayer adsorption.

The mean values of the free energy (E) (Eq. S4) estimated from the Dubinin–Radushkevich isotherm were used to assess the nature of the adsorption, and the values in the range 10.14–13.06 kJ/mol were within the energy range for ion-exchange reactions of 8–16 kJ/mol [79]. A similar fit of isotherms to experimental data using linear regression was observed for dyes adsorbed on sewage sludge-rice husk biochar [72] or activated carbon prepared from coal [60], but in both cases the adsorption process was chemical.

As different studies have used different concentrations, dose of adsorbent, temperature and pH range, it is sometimes difficult to make an accurate comparison of monolayer adsorption capacity. The adsorption capacity is increased by increasing the concentration and decreasing the adsorbent dose. The determined and estimated adsorption capacity of the studied compost was similar to that reported for some other biosorbents, such as low-moor peat, wood industry by-products and agro-waste materials, even though the studies were conducted at a solution pH above 7 (Table S4).

Table 6 The isotherm constants for the adsorption of azo dyes on compost

Dyes	DR-81		DB-74		RB-81		RR-198		ABk-194	
Compost dose	50 g/L	20 g/L	50 g/L	20 g/L	50 g/L	20 g/L	50 g/L	20 g/L	50 g/L	20 g/L
Freundlich isotherm										
K_F	0.4764	0.7489	0.6589	1.299	0.7344	1.624	0.1891	0.3739	1.446	2.716
$1/n$	0.4423	0.4461	0.4336	0.3936	0.4578	0.3886	0.5074	0.5002	0.4014	0.3369
R^2	0.9801	0.9822	0.9741	0.9764	0.9928	0.9729	0.9797	0.9836	0.9937	0.9877
SSE	0.6683	4.184	1.771	5.298	3.661	6.144	0.4727	2.611	6.793	8.611
χ^2	0.5243	0.9298	0.9065	1.816	1.712	1.072	0.4003	0.8263	0.2354	2.473
Langmuir isotherm										
q_{exp}	7.81	13.28	9.43	15.97	11.22	18.55	5.06	9.73	12.64	20.76
q_L	8.91	16.09	10.78	17.25	12.95	19.74	6.441	12.64	14.16	20.92
K_L	0.0088	0.0067	0.0114	0.0127	0.0129	0.0161	0.0049	0.0045	0.0376	0.0364
R^2	0.9995	0.9979	0.9986	0.9971	0.9941	0.9977	0.9952	0.9953	0.9981	0.9979
SSE	0.4851	0.8297	0.4897	1.416	0.2603	0.199	0.0221	0.1485	0.2491	0.4791
χ^2	0.3231	1.1328	0.3771	0.846	0.1108	0.486	0.2812	0.5453	0.3139	0.7674
Dubinin-Radushkevich isotherm										
$q_D 10^{-3}$	0.0432	0.0765	0.0377	0.0528	0.0589	0.0719	0.0247	0.0469	0.0771	0.0874
β	0.0042	0.0045	0.0039	0.0035	0.0041	0.0035	0.0048	0.0048	0.0034	0.0029
E	10.89	10.59	11.37	11.87	11.05	11.90	10.15	10.14	12.03	13.06
R^2	0.9899	0.9901	0.9849	0.9969	0.9968	0.9844	0.9893	0.9909	0.9982	0.9937
SSE	0.3467	2.031	0.7312	2.032	1.614	1.635	0.1971	1.381	2.728	2.006
χ^2	0.1753	0.3056	0.2804	0.687	0.8062	0.517	0.1956	0.3587	1.846	1.384
Sips isotherm										
q_S	10.57	18.19	14.05	23.49	14.31	23.26	7.012	12.57	14.08	25.43
K_S	0.0191	0.0108	0.0219	0.0282	0.0176	0.0286	0.0065	0.0044	0.0369	0.0639
m_S	0.6016	0.8476	0.7278	0.6632	0.8733	0.7632	0.9109	1.007	1.012	0.6768
R^2	0.9995	0.9982	0.9997	0.9971	0.9981	0.9981	0.9962	0.9962	0.9997	0.9975
SSE	0.3546	0.5130	0.2725	0.4368	0.0607	0.1281	0.0078	0.1482	0.0799	0.3934
χ^2	0.2030	0.3851	0.085	0.2241	0.0604	0.0983	0.1144	0.2798	0.1035	0.1934

K_F ((mg/g)·(L/mg)$^{1/n}$); q_{exp}, q_L (mg/g); K_L (L/mg); q_D (mol/g); β (mol^2/J^2); E (kJ/mol); q_S (mg/g); K_S (L/mg)^m

Furthermore, it can be concluded that it was also comparable to the adsorption capacity of activated carbon, but only for DR-81 [80, 81].

Conclusions

The results show that compost, a material rich in organic matter obtained from agricultural waste through the material recovery process, is an important "green adsorbent" in water remediation. It is efficient, low cost, widely available, and easy to use as it does not require any prior treatment (except drying and screening) of the material for the removal of anionic azo dyes (belonging to the monoazo, disazo and trisazo class: DR-81, DB-74, RB-81, RR-198 and ABk-194) from water. The compost has a good buffering capacity and can neutralize acidic wastewater during adsorption without further pH adjustment for already treated waters.

This study showed that the equilibrium time of the dye adsorption process, the adsorption capacity of the compost and the dye removal efficiency depended on the dye structure and its initial concentration in the solution.

The monoazo dyes RB-81, RR-198 and ABk-194 with the smaller particle size were adsorbed the fastest. The dye adsorption rate was high due to the large surface area and pore volume of the compost, indicating that the compost had a high efficiency in removing azo dyes, which determines the wastewater-compost contact time in the wastewater treatment process in real practice.

Statistical analysis showed that the experimental adsorption data fitted very well with the PSO model at high initial dye concentration ($C_0 = 500$ mg/L), indicating that chemisorption controlled the adsorption rate, while both the PFO and PSO models described well the adsorption of dyes at their low initial concentration ($C_0 = 50$ mg/L).

The results showed that the Langmuir and Sips models best fit the adsorption system with maximum adsorption capacities in the range of 12.64 mg/g (RR-198)—20.92 mg/g (ABk-194) and 12.57 mg/g (RR-198)—25.43 mg/g (ABk-194), respectively.

The adsorption depended on the dye structure, especially on the ratio of the number of proton donor (aryl, amino, hydroxyl groups) to proton acceptors (nitro, azo, chloride, sulfate, carbonyl, sulfonylethyl sulfate groups) sites in the functional groups, especially when the adsorption capacity of the compost is expressed in molar units. Chemical reactivity descriptors obtained from the DFT calculations (chemical hardness and electronegativity) showed that the monoazo dyes (ABk-194, RB-81 and RR-198) were more reactive than the dis- and trisazo dyes (DR-81 and DB-74). In addition, electronic density distribution maps showed that dyes with more electron-rich regions were adsorbed in lower amounts on the compost surface than ABk-194 and RB-81 dyes.

The use of composts in water remediation processes is of particular interest for composts that have significant limitations for agronomic purposes (i.e. low nutrient content or above-normative levels of heavy metals), and this is a new green perspective for adsorption science and technology.

Declarations

References

1. Directive 2000/60/EC of the European Parliament and of the council of 23 October 2000 establishing a framework for community action in the field of water policy, special edn. (in Polish), chapter 15, vol. 005, pp. 275–346, http://data.europa.eu/eli/dir/2000/60/oj. Accessed December 2023

2. A. Dzieniszewska, J. Kyziol-Komosinska, M. Pająk, Desal. Water Treat. **177**, 209 (2020). https://doi.org/10.5004/dwt.2020.24933

3. J. Kyziol-Komosinska, C.Z. Rosik-Dulewska, A. Dzieniszewska, M. Pająk, I. Krzyżewska, Environ. Prot. Eng. **40**, 5 (2014). https://doi.org/10.5277/epe140101

4. H.B. Slama, A. Chenari Bouket, Z. Pourhassan, F.N. Alenezi, A. Silini, H. Cherif-Silini, T. Oszako, L. Luptakova, P. Golińska, L. Belbahri, Appl. Sci. **11**, 6255 (2021). https://doi.org/10.3390/app11146255

5. S. Mani, P. Chowdhary, R.N. Bharagava, Emerging and eco-friendly approaches for waste management. In: R. Bharagava, P. Chowdhary (eds) (Springer, Singapore, 2019), pp. 219–244 https://doi.org/10.1007/978-981-10-8669-4_11

6. K. Singh, S. Arora, Crit. Rev. Environ. Sci. Technol. **41**, 807 (2011). https://doi.org/10.1080/10643380903218376

7. K.T. Chung, J. Environ. Sci. Health C Environ. Carcinog. Ecotoxicol. Rev.. **34**, 233 (2016)

8. S. Samsami, M. Mohamadi, M.H. Sarrafzadeh, E.R. Rene, M. Firoozbahr, Process. Saf. Environ. Prot. **143**, 138 (2020). https://doi.org/10.1016/j.psep.2020.05.034

9. R. Khlifi, L. Belbahri, S. Woodward, M. Ellouz, A. Dhouib, S. Sayadi, T. Mechichi, J. Hazard. Mater. **175**, 802 (2010). https://doi.org/10.1016/j.jhazmat.2009.10.079

10. L.D. Paquini, L.T. Marconsini, L.P.R. Profeti, O.S. Campos, D. Profeti, J. Ribeiro, Braz. J. Chem. Eng. **40**, 623 (2023). https://doi.org/10.1007/s43153-023-00300-7

11. P.K. Yeow, S.W. Wong, T. Hadibarata, Biointerface Res. Appl. Chem. **11**, 8218 (2021)

12. S. Afroze, T.K. Sen, Water Air Soil Pollut. **229**, 1 (2018). https://doi.org/10.1007/s11270-018-3869-z

13. A.A. Attia, B.S. Girgis, N.A. Fathy, Dyes Pigm. **76**, 282 (2008). https://doi.org/10.1016/j.dyepig.2006.08.039

14. W. Konicki, M. Aleksandrzak, D. Moszynski, E. Mijowska, J. Colloid Interface Sci. **496**, 188 (2017). https://doi.org/10.1016/j.jcis.2017.02.031

15. J.A. Torres-Luna, G.I. Giraldo-Gómez, N.R. Sanabria-González, J.G. Carriazo, Bull. Mater. Sci. **42**, 137 (2019). https://doi.org/10.1007/s12034-019-1817-1

16. G. Crini, Bioresour. Technol. **97**, 1061 (2006). https://doi.org/10.1016/j.biortech.2005.05.001

17. S. Natarajan, H.C. Bajaj, R.J. Tayade, J. Environ. Sci. **65**, 201 (2018). https://doi.org/10.1016/j.jes.2017.03.011

18. N. Jafarzadeh, A. Takdastan, S. Jorfi, F. Ghanbari, M. Ahmadi, G. Barzegar, J. Mol. Liq. **256**, 462 (2018). https://doi.org/10.1016/j.molliq.2018.02.047

19. O. Türgay, G. Ersoz, S. Atalay, J. Forss, U. Welander, Sep. Purif. Technol. **79**, 26 (2011). https://doi.org/10.1016/j.seppur.2011.03.007

20. T.H. Van, L.H. Nguyen, N.V. Dang, H.P. Chao, Q.T. Nguyen, T.H. Nguyen, T.B.L. Nguyen, D.V. Thanh, H.D. Nguyen, P.Q.

Thang, P.T.H. Thanh, V.P. Hoang, RSC Adv. **11**, 5801 (2021). https://doi.org/10.1039/d0ra09974k

21. K.R. Millington, Advances in Wool Technology. In: N.A.G. Johnson, I.M. Russell (eds) Woodhead Publishing Series in Textiles, Australia, pp. 217–247 (2009). https://doi.org/10.1533/9781845695460.2.217

22. US EPA, United States Environmental Protection Agency database, https://www.epa.gov/eg/effluent-guidelines-database. Accessed December 2023

23. Polish Minister of Maritime Economy and Inland Navigation, Regarding water quality standards for sewage introduced into water or to the ground state of 12 June 2019 (in Polish) (2019)

24. I. Guerrero-Coronilla, L. Morales-Barrera, E. Cristiani-Urbina, J. Environ. Manage. **152**, 99 (2015). https://doi.org/10.1016/j.jenvman.2015.01.026

25. S. De Gisi, G. Lofrano, M. Grassi, M. Notarnicola, Sustain. Mater. Technol. **9**, 10 (2016). https://doi.org/10.1016/j.susmat.2016.06.002

26. G. McKay, M. Hadi, M.T. Samadi, A.R. Rahmani, M.S. Aminabad, F. Nazemi, Desal. Water Treat. **28**, 164 (2011). https://doi.org/10.5004/dwt.2011.2216

27. K. Sushila, A. Sharma, S.C. Sahoo, G. Kumar, S.K. Mehta, R. Kataria, J. Mol. Struct. Struct. **1226**, 129327 (2021). https://doi.org/10.1016/j.molstruc.2020.129327

28. H.I. Chieng, T. Zehra, L.B.L. Lim, N. Priyantha, D.T.B. Tennakoon, Environ. Earth Sci. **72**, 2263 (2014). https://doi.org/10.1007/s12665-014-3135-7

29. P. Janos, P. Michalek, L. Turek, Dyes Pigm. **74**, 363 (2007). https://doi.org/10.1016/j.dyepig.2006.02.017

30. J. Kyziol-Komosinska, C.Z. Rosik-Dulewska, A. Dzieniszewska, M. Pajak, Arch. Environ. Prot. **37/4**, 3 (2011)

31. J. Kyziol-Komosinska, C.Z. Rosik-Dulewska, A. Dzieniszewska, M. Pajak, Fresenius Environ. Bull. **27**, 6 (2018)

32. L. Rusu, M. Harja, A.I. Simion, D. Suteu, G. Ciobanu, L. Favier, Korean J. Chem. Eng. **31**, 1008 (2014). https://doi.org/10.1007/s11814-014-0009-3

33. G. Yuliani, G. Garnier, A.L. Chaffee, J. Water Process Eng. **15**, 43 (2017). https://doi.org/10.1016/j.jwpe.2016.06.004

34. F. Ouazani, H. Benchekor, Y. Chergui, A. Iddou, A. Aziz, J. Environ. Health Sci. Eng. **18**, 1045 (2020). https://doi.org/10.1007/s40201-020-00526-4

35. H. Haffad, M. Zbair, Z. Anfar, H.A. Ahsaine, H. Bouhlal, H. Khallok, Toxin Rev. **40**, 225 (2019). https://doi.org/10.1080/15569543.2019.1584822

36. M.R. Fat'hi, A. Asfaram, A. Hadipour, M. Roosta, J. Environ. Health Sci. Eng. **12**, 62 (2014). https://doi.org/10.1186/2052-336X-12-62

37. S. Yadav, A. Yadav, N. Bagotia, A.K. Sharma, S. Kumar, J. Water Process Eng. **42**, 102148 (2021). https://doi.org/10.1016/j.jwpe.2021.102148

38. G.Z. Kyzas, M. Kostoglou, Mater. (Basel). **7**, 333 (2014). https://doi.org/10.3390/ma7010333

39. R. Paradelo, X. Vecino, A.B. Moldes, M.T. Barral, Environ. Sci. Pollut. Res. **26**, 21085 (2019). https://doi.org/10.1007/s11356-019-05462-x

40. R. Paradelo, K. Al-Zawahreh, M.T. Barral, Materials. **13**, 2179 (2020). https://doi.org/10.3390/ma13092179

41. T. Pushpa, J. Vijayaraghavan, J. Jegan, Desal. Water Treat. **57**, 24368 (2016). https://doi.org/10.1080/19443994.2016.1143405

42. T. Jóźwiak, U. Filipkowska, J. Rodziewicz, A. Mielcarek, D. Owczarkowska, Rocz. Ochr. Srodowiska. **15**, 2411 (2013)

43. T. Pennanen, V. Srivastava, M. Sillanpaa, T. Sainio, J. Clean. Prod. **273**, 122736 (2020). https://doi.org/10.1016/j.jclepro.2020.122736

44. M. Kucbel, H. Raclavská, J. Růžičková, B. Švédová, V. Sassmanová, J. Drozdová, K. Raclavský, D. Juchelková, J. Environ. Manage. **236**, 657 (2019). https://doi.org/10.1016/j.jenvman.2019.02.018

45. I.K. Petrushenko, K.B. Petrushenko, Vacuum **167**, 280 (2019). https://doi.org/10.1016/j.vacuum.2019.06.021

46. T.N.V. De Souza, S.M.L. de Carvalho, M. Gurgel, A. Vieira, M.G.C. da Silva, D.D.S.B. Brasil, Appl. Surf. Sci. **448**, 662 (2018). https://doi.org/10.1016/j.apsusc.2018.04.087

47. A.K. Ghose, A. Pritchett, G.M. Crippen, J. Comput. Chem. **9**, 80 (1988). https://doi.org/10.1002/jcc.540090111

48. R.G. Pearson, Proc. Nat. Acad. Sci. USA **83**, 8440 (1986). https://doi.org/10.1073/pnas.83.22.8440

49. M. Rizvi, N. Tiwari, A. Mishra, R. Gupta, ACS Omega **7**(36), 31667 (2022). https://doi.org/10.1021/acsomega.2c00966

50. H.M.F. Freundlich, J. Phys. Chem. **57**, 385 (1906)

51. I. Langmuir, J. Am. Chem. Soc. **38**, 2221 (1916). https://doi.org/10.1021/ja02268a002

52. M.M. Dubinin, Chem. Rev. **60**, 235 (1960). https://doi.org/10.1021/cr60204a006

53. R. Sips, J. Chem. Phys. **16**, 490 (1948). https://doi.org/10.1063/1.1746922

54. S. Azizian, J. Colloid Interface Sci. **276**, 47 (2004). https://doi.org/10.1016/j.jcis.2004.03.048

55. S. Lagergren, Kungliga Svenska Vetenskapsakademiens Handlingar. **24**(4), 1 (1989)

56. Y.S. Ho, G. McKay, Process Biochem. **34**, 451 (1999). https://doi.org/10.1016/S0032-9592(98)00112-5

57. Y.S. Ho, G. McKay, Process. Saf. Environ. Prot. **76**, 332 (1998). https://doi.org/10.1205/095758298529696

58. H.N. Tran, S.J. You, A. Hosseini-Bandegharaei, H.P. Chao, Water Res. **120**, 88 (2017). https://doi.org/10.1016/j.watres.2017.04.014

59. S. He, X. Liu, P. Yan, A. Wang, J. Su, X. Su, RSC Adv. **9**, 4908 (2019). https://doi.org/10.1039/C8RA10025J

60. S.U. Jan, A. Ahmad, A.A. Khan, S. Melhi, I. Ahmad, G. Sun, C.M. Chen, R. Ahmad, Environ. Sci. Pollut. Res. **28**, 10234 (2021). https://doi.org/10.1007/s11356-020-11344-4

61. K.Y. Foo, B.H. Hameed, Chem. Eng. J. **156**, 2 (2010). https://doi.org/10.1016/j.cej.2009.09.013

62. Regulation (EU) 2019/1009 of the European Parliament and of the Council of 5 June 2019 laying down rules on the making available on the market of EU fertilising products and amending Regulations (EC) No 1069/2009 and (EC) No 1107/2009 and repealing Regulation (EC) No 2003/2003

63. V.V. Gedam, P. Raut, A. Chahande, P. Pathak, Appl Water Sci **9**, 55 (2019). https://doi.org/10.1007/s13201-019-0933-9

64. K. Al-Zawahreh, M.T. Barral, Y. Al-Degs, R. Paradelo, J. Environ. Manage. **294**, 113005 (2021). https://doi.org/10.1016/j.jenvman.2021.113005

65. M. Lawrinenko, D. Jing, C. Banika, D.A. Lairda, Carbon **118**, 422 (2017). https://doi.org/10.1016/j.carbon.2017.03.056

66. J. Kyziol-Komosinska, J. Augustynowicz, W. Lasek, J. Czupioł, D. Ociński, J. Environ. Manage. **214**, 295 (2018). https://doi.org/10.1016/j.jenvman.2018.03.010

67. C. Manera, A.P. Tonello, D. Perondi, M. Godinho, Environ. Technol. **40**, 2756 (2019). https://doi.org/10.1080/09593330.2018.1452984

68. D. Robati, J. Nanostruct. Chem. **3**, 1 (2013). https://doi.org/10.1186/2193-8865-3-55

69. A. Bouguettoucha, D. Chebli, T. Mekhalef, A. Noui, A. Amrane, Desal. Water Treat. **55**, 1956 (2015). https://doi.org/10.1080/19443994.2014.928235

70. W. Plazinski, W. Rudzinski, A. Plazinska, J. Colloid Interface Sci. **152**, 2 (2009). https://doi.org/10.1016/j.cis.2009.07.009

71. J. Chen, H. Hu, J. Yang, H. Xue, Y. Tian, K. Fan, Z. Zeng, J. Yang, R. Wang, Y. Liu, Bioresour. Technol. **322**, 124556 (2021). https://doi.org/10.1016/j.biortech.2020.124556

72. S. Chen, C.X. Qin, T. Wang, F. Chen, X. Li, H. Hou, M. Zhou, J. Mol. Liq. **285**, 62 (2019). https://doi.org/10.1016/j.molliq.2019.04.035

73. M.A.M. Salleh, D.K. Mahmoud, W.A.W.A. Karim, A. Idris, Desalination **280**, 1 (2011). https://doi.org/10.1016/j.desal.2011.07.019

74. Q. He, G. Wang, Z. Chen, Z. Miao, K. Wan, S. Huang, Fuel **267**, 117140 (2020). https://doi.org/10.1016/j.fuel.2020.117140

75. Y. Hu, T. Guo, X. Ye, Q. Li, M. Guo, H. Liu, Z. Wu, Chem. Eng. J. **228**, 392 (2013). https://doi.org/10.1016/j.cej.2013.04.116

76. A. Reife, H.S. Freeman, *Environmental chemistry of dyes and pigments*, 1st edn. (Wiley, New York, 1996)

77. C.H. Giles, D. Smith, A. Huitson, J. Colloid Interface Sci. **47**, 755 (1974). https://doi.org/10.1016/0021-9797(74)90252-5

78. A. Saeed, M. Sharif, M. Iqbal, J. Hazard. Mater. **179**, 564 (2010). https://doi.org/10.1016/j.jhazmat.2010.03.041

79. Q. Hu, Z. Zhang, J. Mol. Liq. **277**, 646 (2019). https://doi.org/10.1016/j.molliq.2019.01.005

80. P. Bhatt, R.K. Vyas, P. Pandit, M. Sharma, Nat. Environ. Pollut. Technol. **12**(3), 397 (2013)

81. N. Sohrabi, N. Rasouli, M. Karimi, J. Sci. Eng. Res. **3**, 46 (2016)

Authors and Affiliations

Joanna Kyziol-Komosinska[1] · **Agnieszka Dzieniszewska[1]** · **Sylwia Pasieczna-Patkowska[2]** · **Anna Kołbus[3]** · **Justyna Czupioł[1]**

✉ Agnieszka Dzieniszewska
agnieszka.dzieniszewska@ipispan.edu.pl

Joanna Kyziol-Komosinska
joanna.komosinska@ipispan.edu.pl

Sylwia Pasieczna-Patkowska
sylwia.pasieczna@poczta.umcs.lublin.pl

Anna Kołbus
anna.kolbus@ujk.edu.pl

Justyna Czupioł
justyna.czupiol@ipispan.edu.pl

[1] Institute of Environmental Engineering, Polish Academy of Sciences, 34 M Skłodowska-Curie St., 41-819 Zabrze, Poland

[2] Department of Chemical Technology, Faculty of Chemistry, University of Maria Curie-Sklodowska, 3 Maria Curie-Sklodowska Square, 20-031 Lublin, Poland

[3] Institute of Chemistry, Jan Kochanowski University, 7 Uniwersytecka Str., 25-406 Kielce, Poland